JACS
JOURNAL OF THE AMERICAN CHEMICAL SOCIETY
Article
pubs.acs.org/JACS

Tuning Polymorphism and Orientation in Organic Semiconductor Thin Films via Post-deposition Processing

Anna M. Hiszpanski,[†] Robin M. Baur,[‡] Bumjung Kim,[§,∥] Noah J. Tremblay,[§,⊥] Colin Nuckolls,[§] Arthur R. Woll,[‡] and Yueh-Lin Loo*[,†]

[†]Department of Chemical and Biological Engineering, Princeton University, A323 Engineering Quadrangle, Princeton, New Jersey 08544, United States

[‡]Cornell High Energy Synchrotron Source, Cornell University, 161 Synchrotron Drive, Ithaca, New York 14853, United States

[§]Department of Chemistry, Columbia University, MC 3130, 3000 Broadway, New York, New York 10027, United States

Supporting Information

ABSTRACT: Though both the crystal structure and molecular orientation of organic semiconductors are known to impact charge transport in thin-film devices, separately accessing different polymorphs and varying the out-of-plane molecular orientation is challenging, typically requiring stringent control over film deposition conditions, film thickness, and substrate chemistry. Here we demonstrate independent tuning of the crystalline polymorph and molecular orientation in thin films of contorted hexabenzocoronene, c-HBC, during post-deposition processing without the need to adjust deposition conditions. Three polymorphs are observed, two of which have not been previously reported. Using our ability to independently tune the crystal structure and out-of-plane molecular orientation in thin films of c-HBC, we have decoupled and evaluated the effects that molecular packing and orientation have on device performance in thin-film transistors (TFTs). In the case of TFTs comprising c-HBC, polymorphism and molecular orientation are equally important; independently changing either one affects the field-effect mobility by an order of magnitude.

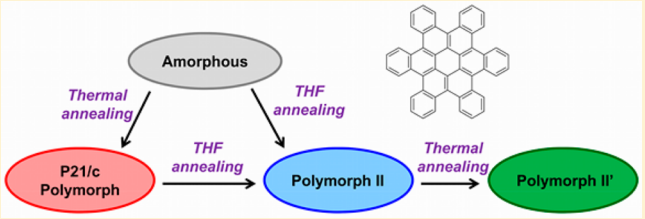

INTRODUCTION

Charge transport in both molecular and polymer-based crystalline organic semiconductors is highly sensitive to molecular packing. For example, even in transistors comprising single crystals of organic semiconductors of pentacene[1] and rubrene,[2] the mobilities can differ by a factor of 3−4 along different crystallographic axes due to molecular anisotropy and differences in the way neighboring molecules are oriented relative to each other. Given the sensitive relationship between molecular packing and charge transport,[3] the ability to alter molecular packing (also known as crystal engineering to the materials community) offers the opportunity to increase the charge carrier mobility of a crystalline molecular semiconductor. Generally, crystal engineering is synonymous with synthesis, where chemical modification of a compound alters molecule−molecule interactions and therefore also molecular packing in the solid-state.[4−7] However, changing the chemical structure necessarily changes the optoelectronic and physical properties of the molecule, such as the energy levels of the material's highest-occupied and lowest-unoccupied molecular orbitals, optical absorptivity, and solubility. This method is also experimentally taxing since at present crystal structure prediction of large (>40 atoms) molecules is difficult,[8,9] and the properties of new crystal structures are challenging to predict *a priori*. Thus, Edisonian cycles of materials synthesis, crystal growth, and characterization, followed by device fabrication and testing, are often required to attain a molecule that, when incorporated in devices, has the desired properties.

Alternatively, crystal engineering without necessitating chemical modification of the parent compound is possible for many small molecules that adopt more than one crystal structure, i.e., molecules that exhibit polymorphism. While polymorphism of molecular crystals has been a long-standing point of interest to the pharmaceutical community,[10,11] where solubility and bioavailability of drugs can vary with the crystalline form, polymorphism of small molecule organic semiconductors has only recently become a growing area of interest with an increasing number of organic semiconductors demonstrating polymorphism.[12−27] The ability to access different polymorphs of a single organic semiconductor provides the opportunity to study the effects of solid-state packing on charge transport, potentially providing access to crystal structures with more favorable electronic properties.[12−14,16,20] For example, devices constructed from single crystals having different polymorphs of tetrathiafulvalene[12] and rubrene[20] have mobilities that differ by a factor of 6 and 10, respectively, and devices composed of single crystals having

Received: September 3, 2014
Published: October 15, 2014

   dx.doi.org/10.1021/ja5091035 | J. Am. Chem. Soc. 2014, 136, 15749−15756

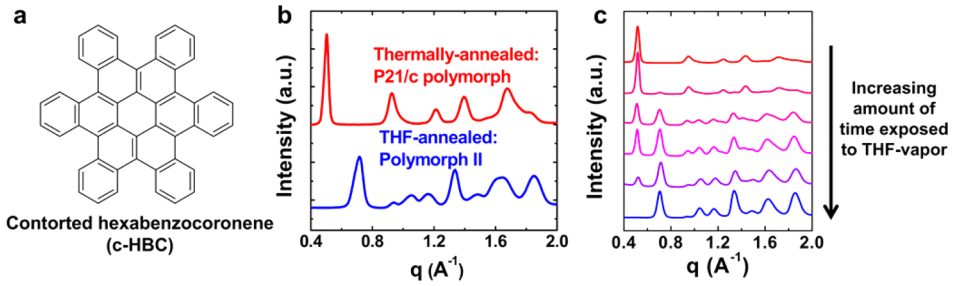

Figure 1. (a) Chemical structure of contorted c-HBC, an organic semiconductor demonstrating hole-transport. (b) One-dimensional "powder" diffraction traces (generated by azimuthally integrating two-dimensional grazing-incidence X-ray diffraction images) of the two polymorphs accessed by either thermally annealing an amorphous c-HBC film at 240 °C for 30 min, resulting in a polymorph with the $P2_1/c$ space group, or THF-vapor annealing for 4 h, resulting in a new, unknown crystal structure, termed polymorph II. (c) Diffraction traces of a thermally annealed film irreversibly transforming *ex-situ* from the $P2_1/c$ polymorph to polymorph II with an increasing amount of time having been exposed to THF-vapor.

distinct polymorphs of dithiophene-tetrathiafulvalene (DT-TTF) show differences in mobilities between a factor of 2 and 10 depending on the device geometry employed.[13]

Though polymorphism has been observed in a number of organic semiconductors,[12−27] reproducibly accessing other polymorphic forms, particularly in polycrystalline thin films, remains an unmet challenge. In the above-mentioned cases, the different polymorphs were attained by growing single crystals from different solvents. In thin films, controllably accessing different crystalline phases is more challenging, often requiring stringent deposition method and conditions, film thickness, and substrate chemistry.[13,27−29] For example, pentacene has four polymorphs, but to access each in thin films requires a specific film thickness, substrate choice, and substrate temperature during deposition.[15,17,30] Likewise, the metastable polymorph of 6,13-bis(triisopropylsilylethynyl) pentacene (TIPS-pentacene) is only accessible when the film is deposited using a solution shearing method,[16,31] ideally with a blade having patterned micropillars.[32]

Here, we report the ability to access three different polymorphs of contorted hexabenzocoronene (c-HBC; chemical structure in Figure 1a) thin films, two of which have not been previously reported, using only post-deposition processing.[33] We have been able to traverse the rich phase space of c-HBC using the repeated application of thermal and solvent-vapor annealing, common and simple post-deposition processing treatments, without requiring any modification of the underlying substrate or specifications of the film deposition conditions or film thickness. Our ability to access such a diverse phase space stems from the fact that we induce crystallization after film formation from a kinetically trapped, amorphous solid-state. By altering the sequence of thermal and solvent-vapor annealing, we can independently tune the crystal structure and the distribution of out-of-plane molecular orientation in c-HBC thin films, allowing us to decouple the relative contribution of each to charge transport in thin-film transistors.

RESULTS AND DISCUSSION

A hole-transporting organic semiconductor[34,35] and polycyclic aromatic hydrocarbon,[36,37] c-HBC is a molecule of interest due to its highly nonplanar shape, which has been reported to readily complex with fullerene derivatives for use in organic solar cells given their shape complementarity.[38,39] We previously reported that different post-deposition processing treatments, including hexanes solvent-vapor annealing, thermal annealing, and physical contact with a cured silicone elastomeric stamp, induces crystallization of amorphous c-HBC films with increasing extents of out-of-plane molecular orientation.[35] Though the molecular orientation of c-HBC differed with treatment, all three of these treatments induced crystallization of the c-HBC films in the same monoclinic polymorph having a $P2_1/c$ space group. This molecular packing is shown in Supporting Information Figure S1a. In an effort to access a greater range of out-of-plane molecular orientations, we investigated post-deposition annealing of c-HBC films with other solvent vapors and found, surprisingly, that some solvent vapors, such as tetrahydrofuran (THF), induce the formation of a previously unreported crystal structure. The 2D grazing-incidence X-ray diffraction (2D-GIXD) image of a THF-annealed film adopting this new polymorph is shown in Figure 2a. To most easily identify differences in the X-ray diffraction patterns that result from these two polymorphs, we show in Figure 1b the azimuthally integrated X-ray traces of thermally annealed and THF-vapor annealed films adopting the $P2_1/c$

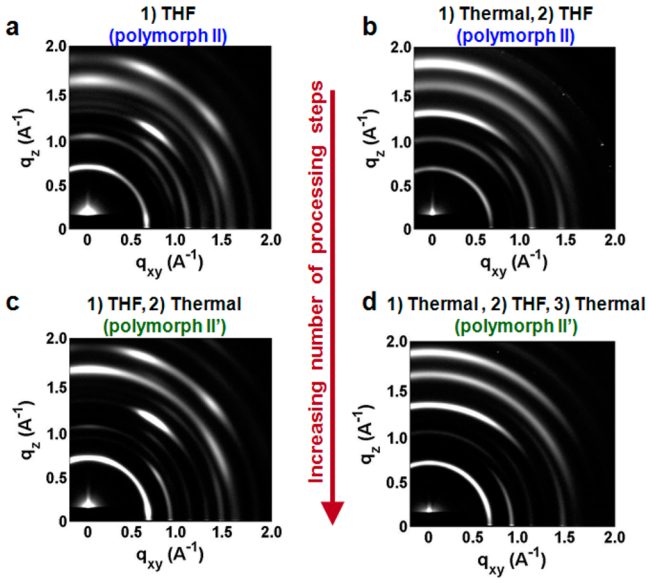

Figure 2. 2D-GIXD images of c-HBC thin films after (a) THF-annealing and (b) thermal- and THF-annealing, resulting in both films adopting polymorph II albeit with different texturing. (c, d) Further processing each of these films with an additional thermal-annealing step results in them both transforming to polymorph II′, as is evidenced by the inversion in the relative intensities of peaks in the q = 0.9−1.2 Å^{-1} range and the change of reflections to slightly larger q-spacing.

dx.doi.org/10.1021/ja5091035 | J. Am. Chem. Soc. 2014, 136, 15749−15756

polymorph and the new polymorph, respectively. The most notable difference between these X-ray traces is in the placements of the primary reflections that occur at q = 0.51 Å^{-1} for the $P2_1/c$ polymorph and at q = 0.68 Å^{-1} for the new polymorph.

Attempts to grow single crystals of the new polymorph in order to determine its crystal structure were unsuccessful. In general, growing single crystals from solution or from physical-vapor transport can be difficult, requiring exact and stringent coincidence of appropriate physical conditions. Growing crystals from chlorobenzene resulted in an orthorhombic polymorph of c-HBC having the *Pbcn* space group (Supporting Information Figure S1b), but the diffraction from the *Pbcn* polymorph does not match that of the new polymorph that we accessed through THF-vapor annealing of c-HBC thin films (Supporting Information Figure S1c). The difficulty in obtaining single crystals of the new polymorph could arise from two causes: either we have not accessed the right growth conditions, or this polymorph only exists in thin films. Indeed, pentacene,[30,40−42] thiotetracene,[43] and *N*,*N*′-dioctyl-3,4:9,10-perylene tetracarboxylic diimide[44] have been reported to exhibit unique polymorphs that only exist when the films are below a material-specific critical thickness that is generally below 50 nm; we maintained a constant thickness of ca. 110 nm in our studies. We have also tried to extract the unit cell lattice parameters of the new polymorph from its thin-film diffraction pattern recognizing that this endeavor, too, is challenging given the limited number of unique reflections and the breadths of these reflections in our patterns. For comparison, single-crystal diffraction usually yields over 5000 reflections, of which over 1000 are unique. While this effort also did not yield a unique crystal structure, comparison of this X-ray diffraction pattern with others generated in the DPC toolkit[45] and powder-diffraction autoindexing programs[46] suggests that it belongs to the triclinic crystal system. We refer to this new polymorph as polymorph II. While this paper only details THF-vapor annealing as a means of accessing polymorph II, we have also been able to access the crystal structure that gives rise to the same X-ray diffraction pattern by solvent-vapor annealing with yet other solvents, including dichloromethane and trichloroethylene. Given this observation, it is unlikely that polymorph II is the result of crystallization of c-HBC and THF.

In addition to accessing polymorph II directly from amorphous films, subjecting thermally annealed c-HBC films that already adopt the $P2_1/c$ crystal structure to THF vapors induces this transformation as well. Figure 1c contains the evolution of the azimuthally integrated X-ray diffraction traces, tracking the primary reflections as a c-HBC film exhibiting the $P2_1/c$ polymorph is exposed to THF vapors. We observe that the primary peak associated with the $P2_1/c$ polymorph at q = 0.51 Å^{-1} attenuates in intensity and disappears while the primarily peak associated with polymorph II at q = 0.68 Å^{-1} emerges. Figure 2b shows the 2D-GIXD image of the twice-treated c-HBC film after its transformation to polymorph II is complete. Azimuthally integrating the GIXD images of the THF-annealed film (Figure 2a) and the thermally annealed and then THF-vapor annealed film (Figure 2b) produces comparable diffraction traces, shown in Figure 3a,b, respectively, indicating that we can access polymorph II with both processing routes. While these films adopt the same polymorph, differences in processing routes do impart differences in the azimuthal distribution of intensities in the 2D-GIXD images in Figure 2a,b. Since the azimuthal

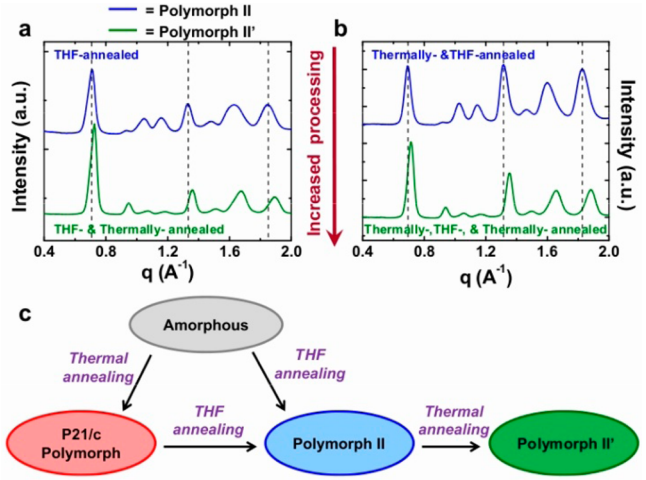

Figure 3. "Powder" diffraction patterns generated from azimuthally integrating 2D-GIXD images of c-HBC films that were first either (a) THF-annealed or (b) thermally annealed and then THF-annealed, resulting in the films adopting polymorph II (blue traces). Subjecting each of these films to an additional thermal annealing step results in their transformation to polymorph II′ (green traces). The dashed vertical lines are provided as a guide for the eye to better discern differences between polymorph II and II′. (c) A schematic summarizing the processing techniques applied and crystal structures accessed as a result.

distribution of intensities in 2D-GIXD images is a direct indication of crystal orientation, the difference observed between parts a and b of Figures 2 suggests that c-HBC is oriented differently in these films despite adopting the same molecular packing. Figure 4a presents pole figures for the two

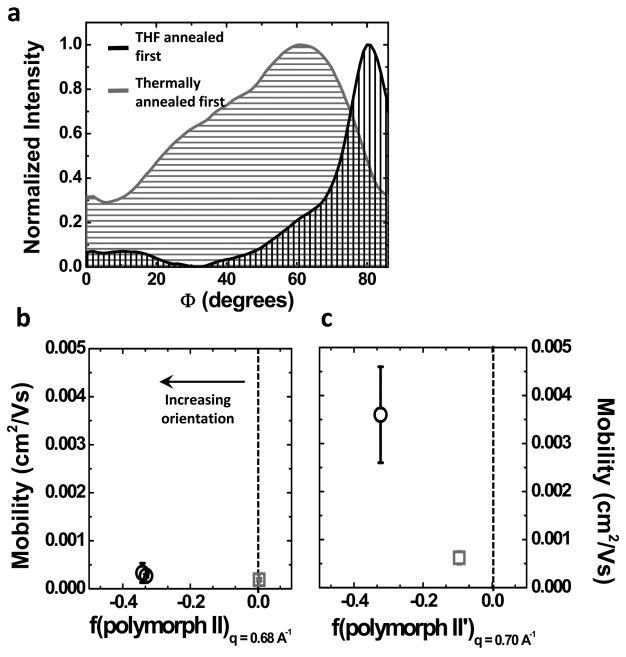

Figure 4. (a) Pole figure constructed by tracking the azimuthal intensity of the q = 0.68 Å^{-1} reflection of polymorph II-containing films that were either thermally annealed and then THF-annealed (gray trace) or only THF-annealed (black trace). The mobility plotted as a function of Herman's orientation function, f, for thin-film transistors constructed with (b) polymorph II and (c) polymorph II′ films.

dx.doi.org/10.1021/ja5091035 | J. Am. Chem. Soc. 2014, 136, 15749−15756

polymorph II-containing films under discussion; the black trace corresponds to the pole figure of the c-HBC film that was only THF-vapor annealed whereas the gray trace corresponds to that of the film that was thermally annealed and then THF-vapor annealed. The pole figures were constructed by tracking the intensity of the reflection at q = 0.68 Å^{-1} along the azimuthal angle, where 0° is normal to the substrate. The intensity distribution of this reflection of the THF-vapor annealed film is centered at 80°, indicating that the crystallographic plane associated with this reflection is oriented almost normal to the substrate. Furthermore, the intensity is narrowly distributed about 80°, reflecting a narrow distribution of orientation. Conversely, the intensity distribution of the same reflection extracted from the pole figure of the thermally annealed and then THF-vapor annealed film is much broader, indicating that this film exhibits a much broader distribution of orientation.

The degree of orientation can be quantified using Herman's orientation function, f.[35] f can range between 1 and −0.5, where f = 1 occurs when the intensity of the reflection of interest is entirely concentrated at 0°, f = −0.5 occurs when the same intensity is concentrated at 90°, and f = 0 occurs when the intensity is isotropically distributed along the azimuthal angle and thus implies no preferential orientation. Performing this analysis on the pole figures shown in Figure 4a yields f = −0.34 for the THF-vapor annealed film and f = 0 for the c-HBC film that had undergone both thermal annealing and then THF-vapor annealing. Thus, while polymorph II can be accessed by both THF-vapor annealing an amorphous c-HBC film and by THF-vapor annealing a thermally annealed film that adopts the $P2_1/c$ polymorph, the more oriented film is only accessed by the former processing route.

Given that we can access polymorph II by THF-vapor annealing a thermally annealed $P2_1/c$ film, we carried out the processing in the opposite sequence to assess reversibility, starting instead with a THF-vapor annealed, polymorph II film and thermally annealing it. Figure 2c shows the 2D-GIXD image of a THF-vapor annealed film after it had undergone an additional thermal annealing step. That the primary reflection at q = 0.51 Å^{-1} remains absent indicates that the film did not transform back to the $P2_1/c$ polymorph on thermal annealing. It thus appears that while we can transform films having the $P2_1/c$ crystal structure to polymorph II, this process is not reversible.

However, on closer inspection, the GIXD pattern in Figure 2c does exhibit subtle differences when compared to the diffraction image in Figure 2a. These differences are most readily apparent in their one-dimensional diffraction traces shown in Figure 3a. Specifically, we observe that the peaks in the X-ray diffraction trace obtained on the THF-vapor and then thermally annealed film are located at larger q's compared to those in the X-ray diffraction trace of the starting film that was only THF-vapor annealed. The primary peak, in particular, is located at q = 0.70 Å^{-1} in the THF-vapor and thermally annealed film, as opposed to its location at q = 0.68 Å^{-1} in the starting film that was only a THF-vapor annealed film. The change in peak positions upon thermally annealing the THF-vapor annealed film is even more apparent at higher q-spacing. This increase in q-spacing is suggestive of a decrease in the lattice parameters of the crystal unit cell. Thus, while we cannot access the $P2_1/c$ crystal structure from films having polymorph II, subsequent thermal annealing yields yet a different polymorph whose unit cell dimensions are slightly smaller than those of polymorph II. Given the qualitative similarity in the X-ray diffraction pattern, we shall refer to this polymorph as polymorph II′. Further evidence that polymorph II′ is yet different from polymorph II stems from relative intensity differences in the X-ray diffraction traces. The intensities of reflections at q = 1.05 and 1.15 Å^{-1} are substantially attenuated in the X-ray diffraction trace of polymorph II′ compared to that of polymorph II. This intensity attenuation is accompanied by a concomitant intensity increase of the reflection at q = 0.93 Å^{-1}. Such differences in the relative intensities of reflections indicate differences in the structure factor that arise from changes in intermolecular packing between the two polymorphs. Unfortunately, without identification of the crystal structure, we are not able to elucidate such differences. There are, however, important details we can learn by comparing the X-ray diffraction patterns of the two polymorphs. Given the similarities in the X-ray diffraction patterns and the proximity in the majority of the reflections, we believe polymorph II′, like polymorph II, belongs to the triclinic crystal system, likely with closely related lattice parameters but with molecules shifted relative to one another in their packing. Such closely related polymorphs are common; pentacene's four identified triclinic polymorphs similarly show small differences in their powder diffraction patterns as a result of the small differences in their lattice parameters. Yet, these polymorphs each have notable differences in their intermolecular packing.[17,47] More recently, strained polymorphs of TIPS-pentacene[16,32] and 2,7-dioctyl[1]-benzothieno[3,2-*b*][1]benzothiophene[29] have also been reported, where strain induced during film deposition slightly alters the intermolecular packing. We hesitate to refer to polymorphs II and II′ as strained polymorphs as these polymorphs were accessed in the absence of an external field.

We have tracked the transformation of polymorph II to II′ by performing *in-situ* 2D-GIXD experiments at the G1-line of Cornell High Energy Synchrotron Source using a custom "SabreTube" furnace (Absolute Nano, Wixom, MI) that consists of a suspended heated silicon platform allowing for rapid heating[48] whose read-out temperature has been calibrated against indium, tin, and lead standards. We chose to use the simultaneous intensity increase and decrease of reflections at q = 0.93 Å^{-1} and 1.05 Å^{-1}, respectively, to track the progression of transformation from polymorph II to II′. Focusing on this region of interest, Figure 5a shows the diffraction traces of a THF-annealed film transforming from polymorph II to II′ at 244 °C. The diffraction trace of the first 2D-GIXD image (red curve in Figure 5a) denotes time = 0 and was taken at room

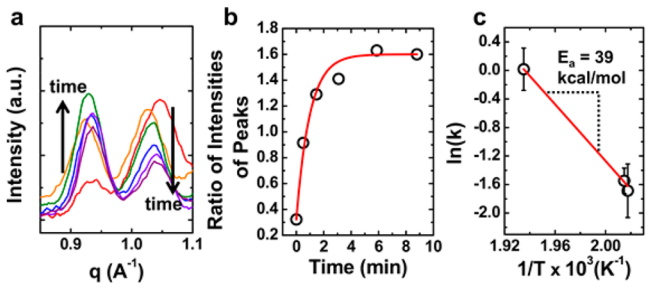

Figure 5. (a) Diffraction traces showing the region of interest for tracking *in-situ* the transformation from polymorph II to II′ at 244 °C of a THF-vapor annealed c-HBC film. (b) The transformation was tracked by the ratio of intensities of the reflections at q = 0.93 and 1.05 Å^{-1} and fitted to a first-order Avrami kinetics model. (c) An Arrhenius plot yielding an energy barrier to transformation of 39 kcal/mol.

dx.doi.org/10.1021/ja5091035 | J. Am. Chem. Soc. 2014, 136, 15749−15756

temperature. The sample is rapidly heated to 244 °C; we estimate that the sample reaches the target temperature within 10 s. The initial decrease in the q-spacing of reflections at q = 0.93 and 1.05 Å^{-1} is due to thermal expansion of the crystal lattice. The peaks subsequently shift to larger q-spacing with time, as is expected with the transformation from polymorph II to II′. Figure 5b shows the ratio of intensities of the reflections at q = 0.93 and 1.05 Å^{-1} as a function of time; the transformation is well described by first-order Avarami kinetics[49,50] from which the rate constant, k, can be extracted. Performing a series of such isothermal transformation experiments yielded an energy barrier to transformation of 39 kcal/mol (see Figure 5c). To our knowledge, this is the first report of an energy barrier between polymorphs in an organic semiconductor system. For comparison, the energy barrier for transformation between polymorphic forms of small-molecule drugs of nimodipine and indomethacin is approximately 2 and 13 kcal/mol,[51] respectively, while the polymorphic transformation of titania from brookite to rutile has an activation energy barrier of approximately 100 kcal/mol.[52]

Returning to Figure 2a,c, we note that the azimuthal intensity distributions appear comparable in the two GIXD patterns, suggesting that we can access films of polymorphs II and II′ having comparable molecular orientations. This assertion can be further verified by comparing the pole figures extracted from these GIXD patterns (see Supporting Information Figure S5b) and quantified by calculating the Herman's orientation functions for the two films. Our analysis yielded f = −0.34 for the THF-vapor annealed film comprising polymorph II and f of −0.32 for the film that had been subjected to an additional thermal annealing step in order to transform to polymorph II′. These values indicate that, despite having different crystal structures, the two films exhibit comparable textures.

To determine if polymorph II′ may be accessed regardless of the film's processing history, we also took the twice-treated, thermally annealed and THF-vapor annealed film that had been transformed from the $P2_1/c$ crystal structure to polymorph II (Figure 2b), and we subjected it to a third thermal annealing step, producing the 2D-GIXD image shown in Figure 2d. Though qualitatively the image appears similar to that of the twice-treated, polymorph II-containing film, a comparison of the diffraction traces, shown in Figure 3b, elucidates differences. Upon the third processing step of thermal annealing, the diffraction pattern is shifted to larger q-spacing and shows a similar inversion of the relative intensities associated with reflections in the q-range of 0.9 to 1.2 Å^{-1}, indicating transformation from polymorph II to polymorph II′. This transformation is consistent with the polymorph II to II′ transformation that occurred upon thermally annealing the only once-treated THF-vapor annealed film; our experiments thus indicate that, regardless of the method by which polymorph II is accessed, whether directly by THF-vapor annealing an amorphous c-HBC film or by THF-vapor annealing a c-HBC film that exhibits the $P2_1/c$ polymorph after thermal annealing, subsequent thermal annealing always yields polymorph II′. The pole figures generated from the 2D-GIXD images of the twice- and thrice-treated films are shown in Supporting Information Figure S5a.The thrice-treated film has an f = −0.09, compared to that of the twice-treated film, at f = 0, indicating that the film has become slightly more textured upon thermal annealing as a third processing step.

For clarity, we have summarized in Figure 3c the processing flow diagram that has allowed us to access polymorphs II and II′. The preferred out-of-plane molecular orientation adopted by c-HBC appears to be dictated by the first processing step; with two processing routes to access polymorph II, we can access films with the same crystal structure but different extents of preferential orientation. Furthermore, subjecting films exhibiting polymorph II to thermal annealing transforms them to polymorph II′ without imposing changes to the molecular orientation, thus providing films exhibiting the same preferred molecular orientation but different crystal structures. This possibility, made possible through sequential post-deposition processing, allows us to assess the relative impact that polymorphism and molecular orientation in polycrystalline c-HBC thin films have on films' electronic properties through the construction of thin-film transistors (TFTs).

Top-contact, bottom-gate devices were constructed by thermally evaporating c-HBC on hexamethyldisilazane-treated silicon substrates with a thermally grown 300 nm oxide layer. After post-deposition processing treatments were applied, 60 nm-thick Au source and drain contacts were evaporated through a stencil mask, defining channels having 100 μm lengths and 2000 μm widths. Supporting Information Table S1 summarizes the device characteristics. Saturated field-effect mobilities were calculated, and the threshold voltages were determined by linear extrapolation from the saturation transfer curves. On/off ratios were calculated from transfer curves taking the current at V_G = −100 V to be "on" and the current at V_G = 0 V to be "off". Representative transfer curves are provided in Figure S6 of Supporting Information.

We previously demonstrated in studies involving crystalline films of c-HBC having the $P2_1/c$ crystal structure that differences in the preferred out-of-plane orientation could affect field-effect mobilities in polycrystalline thin-film transistors by an order of magnitude.[35] To compare the mobilities of devices comprising polymorphs II and II′, we have plotted them as a function of Herman's orientation function. Figure 4b shows the mobilities as a function of Herman's orientation function extracted from films having polymorph II. We accessed polymorph II by either THF-vapor annealing, by thermally annealing followed by THF-vapor annealing, or by THF-vapor annealing of a film that had been THF-vapor then thermally annealed. We see that regardless of the variation in orientation as quantified by the Herman's orientation function, the field-effect mobilities of devices having films that exhibit polymorph II have low mobilities, on the order of 2−4 × 10^{-4} cm^2/(V s). Figure 4c is the analogous figure for devices comprising polymorph II′. In comparing the mobilities of devices constructed with films of polymorph II′ having different orientations, we note the mobility increases by a factor of 6 with increasing preferential orientation. This increase in mobility with increasing preferential orientation is similar to what we previously observed with devices having the $P2_1/c$ polymorph where the field-effect mobilities increased by an order of magnitude with increasing extents of out-of-plane orientation. If we then compare the mobilities of devices constructed with films of polymorphs II and II′ having the same orientation, i.e., $f \approx -0.3$, we note that devices containing films of polymorph II′ have an order of magnitude higher mobilities than devices with films of polymorph II, indicating that polymorph II′ transports charge more effectively than polymorph II by up to an order of magnitude.

Attributing differences in field-effect mobility to changes in crystal structures is generally challenging with active layers having polycrystalline thin films as this quantity is a reflection of

dx.doi.org/10.1021/ja5091035 | J. Am. Chem. Soc. 2014, 136, 15749−15756

both inter- and intragrain charge transport, and is most often limited by intergrain transport. Previous methods to access different polymorphic films have required altering the deposition method or substrate, both of which can affect other characteristics of film morphology, including the grain size. As such, differences in intergrain transport can complicate analysis. Different from past reports, we have been able to uniquely access different polymorphs while maintaining near-constant grain size and molecular orientation through sequential post-deposition processing of the same film, with which we have been able to draw direct correlations between the polymorph accessed and the performance of devices comprising that polymorph. To further rule out mobility differences due to grain size coarsening,[53,54] we characterized the films after each treatment using atomic force microscopy, AFM. Separately, we estimated the ensemble-average correlation lengths, or the average distances across which the crystalline order is preserved,[55] across all these films based on the 2D-GIXD patterns collected. The analysis and results, which are provided in Supporting Information (see Figures S7 and S8, Table S1), show that the variations in grain size and correlation lengths between polymorph II and II′ are generally less than a factor of 2. As such, we do not believe domain coarsening to be a major contributor to the differences in field-effect mobility reported herein for devices having polymorphs II and II′. Furthermore, in agreement with our results, transistors fabricated from single crystals of different polymorphs of other organic semiconductors also show approximately an order of magnitude difference in mobility.[12,13,20] These differences in mobility arising from variations in crystal structure are of a similar order of magnitude to the observed mobility anisotropy along different crystallographic axes within single crystals of pentacene[1] and rubrene.[2]

As we are able to access both polymorph II and II′ in c-HBC thin films and independently vary the extents of orientation and without necessitating changes to the substrate or deposition technique, we have been able to decouple and quantify the contributions of crystal structure and orientation in improving field-effect mobilities of c-HBC thin-film transistors. Our findings show that having the appropriate crystal structure and having a high extent of preferred orientation can each impact the field-effect mobility by approximately an order of magnitude. In concert, these results suggest that the electronic properties of molecular semiconductors are highly sensitive to differences in molecular packing, be they changes in unit cell dimensions and crystal structure or local variations in the molecules' orientation relative to one another.

CONCLUSIONS

Applying multistep post-deposition processing to amorphous c-HBC films has allowed us to access a rich phase space and tune both the crystal structure and the out-of-plane preferential molecular orientation in c-HBC thin films. By applying two simple post-deposition processing techniques, thermal and solvent-vapor annealing, alternatingly, we were able to create films having the same crystal structure and different out-of-plane orientations, or, the same out-of-plane orientation but different crystal structures. Though the field-effect mobilities of our devices are less than those of devices comprising state-of-the-art molecular semiconductors, our work demonstrates remarkable tunability over both crystal structure and film texture and marks the first decoupling and quantification of the relative contribution of these two variables to the field-effect mobilities of polycrystalline thin films. Our results indicate that even slight changes in crystal structure, as is the case between polymorph II and its related counterpart, polymorph II′, can affect the field-effect mobilities of thin-film transistors by up to an order of magnitude. This difference in mobility is on par with improvements in mobility that are attained by accessing a more favorable out-of-plane molecular orientation. We believe that sequential post-deposition processing with thermal and solvent-vapor annealing, among other techniques, will offer an easily applicable means of tuning each of these factors.

To explore the degree of polymorphic control attainable, we also tried solvent-vapor annealing c-HBC with a number of other solvents in addition to THF. Depending on the solvent, we can crystallize c-HBC films having purely the $P2_1/c$ polymorph, purely polymorph II, or, in certain cases, such as when solvent-vapor annealing with nitroethane or benzene, a mixture of $P2_1/c$ and polymorph II. Access to each polymorph depends on both thermodynamic and kinetic parameters and stems from the subtle interplay between intermolecular and molecule−solvent interactions, as well as the rate at which crystallization takes place. We are currently exploring this parameter space to better understand the variables governing polymorph selection. We believe we have been able to access the rich phase space of c-HBC in large part because structure development in these thin films is decoupled from film formation. By decoupling the film formation and crystallization processes, the kinetics of crystallization and the subtle interplay between molecule−molecule and molecule−solvent interactions that dictate which crystalline phase is accessed can be better manipulated. Furthermore, we have observed that this technique is more widely applicable than to c-HBC; we have similarly accessed a greater polymorph phase space with other compounds, including those with and without coronene cores, by starting with a kinetically trapped amorphous film and subsequently inducing crystallization with post-deposition processing techniques. By further exploring the relationship between processing and crystal structure and, likewise, the relationship between crystal structure and charge transport of small molecule organic semiconductors, more rational processing techniques to improve device performance will be developed.

ASSOCIATED CONTENT

Supporting Information

Details regarding synthesis and experimental procedures; table summarizing films' structural characteristics and corresponding devices' performance; crystal structures, including CIF data; 2D-GIXD images in polar coordinates; resolved diffraction traces; kinetics of polymorph II to II′ transformation; complete set of pole figures; TFT transfer characteristics; AFM images. This material is available free of charge via the Internet at http://pubs.acs.org.

AUTHOR INFORMATION

Corresponding Author

lloo@princeton.edu

Present Addresses

[‖]Department of Chemistry, New Jersey City University, Jersey City, New Jersey.

[⊥]Nano-Terra LLC, Brighton, Massachusetts.

Notes

The authors declare no competing financial interest.

■ ACKNOWLEDGMENTS

This work was supported by the NSF MRSEC program through the Princeton Center for Complex Materials (DMR-0819860) and the SOLAR Initiative at the NSF (DMR-10135217). GIXD experiments were conducted at CHESS, which is supported by NSF and NIH/NIGMS under award DMR-0936384. A.M.H. acknowledges support through the National Defense Science and Engineering Graduate (NDSEG) Fellowship (Air Force Office of Scientific Research 32 CFR 168a). We thank Aaron and Wesley Sattler of the Parkin Group (Columbia University) for solving the HBC crystal structures, and we also thank Detlef Smiglies and Nan Yao for helpful discussions.

■ REFERENCES

(1) Lee, J. Y.; Roth, S.; Park, Y. W. *Appl. Phys. Lett.* **2006**, *88*, 252106.
(2) Sundar, V. C.; Zaumseil, J.; Podzorov, V.; Menard, E.; Willett, R. L.; Someya, T.; Gershenson, M. E.; Rogers, J. A. *Science* **2004**, *303*, 1644−1646.
(3) Bredas, J. L.; Calbert, J. P.; da Silva, D. A.; Cornil, J. *Proc. Natl. Acad. Sci. U.S.A.* **2002**, *99*, 5804−5809.
(4) Anthony, J. E.; Brooks, J. S.; Eaton, D. L.; Parkin, S. R. *J. Am. Chem. Soc.* **2001**, *123*, 9482−9483.
(5) Anthony, J. E.; Subramanian, S.; Parkin, S. R.; Park, S. K.; Jackson, T. N. *J. Mater. Chem.* **2009**, *19*, 7984−7989.
(6) Sheraw, C. D.; Jackson, T. N.; Eaton, D. L.; Anthony, J. E. *Adv. Mater.* **2003**, *15*, 2009−2011.
(7) Mas-Torrent, M.; Hadley, P.; Bromley, S. T.; Ribas, X.; Tarres, J.; Mas, M.; Molins, E.; Veciana, J.; Rovira, C. *J. Am. Chem. Soc.* **2004**, *126*, 8546−8553.
(8) Price, S. L. *Phys. Chem. Chem. Phys.* **2008**, *10*, 1996−2009.
(9) Bardwell, D. A.; Adjiman, C. S.; Arnautova, Y. A.; Bartashevich, E.; Boerrigter, S. X. M.; Braun, D. E.; Cruz-Cabeza, A. J.; Day, G. M.; Della Valle, R. G.; Desiraju, G. R.; van Eijck, B. P.; Facelli, J. C.; Ferraro, M. B.; Grillo, D.; Habgood, M.; Hofmann, D. W. M.; Hofmann, F.; Jose, K. V. J.; Karamertzanis, P. G.; Kazantsev, A. V.; Kendrick, J.; Kuleshova, L. N.; Leusen, F. J. J.; Maleev, A. V.; Misquitta, A. J.; Mohamed, S.; Needs, R. J.; Neumann, M. A.; Nikylov, D.; Orendt, A. M.; Pal, R.; Pantelides, C. C.; Pickard, C. J.; Price, L. S.; Price, S. L.; Scheraga, H. A.; van de Streek, J.; Thakur, T. S.; Tiwari, S.; Venuti, E.; Zhitkov, I. K. *Acta Crystallogr., Sect. B* **2011**, *67*, 535−551.
(10) *Polymorphism: In the Pharmaceutical Industry*; Hilfiker, R., Ed.; Wiley-VCH Verlag: Weinheim, Germany, 2006.
(11) Bernstein, J. *Polymorphism in Molecular Crystals*, 1st ed.; Oxford University Press: Oxford, 2008.
(12) Jiang, H.; Yang, X. J.; Cui, Z. D.; Liu, Y. C.; Li, H. X.; Hu, W. P.; Liu, Y. Q.; Zhu, D. B. *Appl. Phys. Lett.* **2007**, *91*, 123505.
(13) Pfattner, R.; Mas-Torrent, M.; Bilotti, I.; Brillante, A.; Milita, S.; Liscio, F.; Biscarini, F.; Marszalek, T.; Ulanski, J.; Nosal, A.; Gazicki-Lipman, M.; Leufgen, M.; Schmidt, G.; Molenkamp, L. W.; Laukhin, V.; Veciana, J.; Rovira, C. *Adv. Mater.* **2010**, *22*, 4198−4203.
(14) Jurchescu, O. D.; Mourey, D. A.; Subramanian, S.; Parkin, S. R.; Vogel, B. M.; Anthony, J. E.; Jackson, T. N.; Gundlach, D. J. *Phys. Rev. B* **2009**, *80*, 085201.
(15) Mattheus, C. C.; Dros, A. B.; Baas, J.; Meetsma, A.; Boer, J. L. d.; Palstra, T. T. M. *Acta Crystallogr., Sect. C* **2001**, *57*, 939−941.
(16) Giri, G.; Verploegen, E.; Mannsfeld, S. C. B.; Atahan-Evrenk, S.; Kim, D. H.; Lee, S. Y.; Becerril, H. A.; Aspuru-Guzik, A.; Toney, M. F.; Bao, Z. *Nature* **2011**, *480*, 504−508.
(17) Mattheus, C. C.; Dros, A. B.; Baas, J.; Oostergetel, G. T.; Meetsma, A.; de Boer, J. L.; Palstra, T. T. M. *Synth. Met.* **2003**, *138*, 475−481.
(18) Law, K. Y. *Chem. Rev.* **1993**, *93*, 449−486.
(19) Huang, L. W.; Liao, Q.; Shi, Q.; Fu, H. B.; Ma, J. S.; Yao, J. N. *J. Mater. Chem.* **2010**, *20*, 159−166.
(20) Matsukawa, T.; Yoshimura, M.; Sasai, K.; Uchiyama, M.; Yamagishi, M.; Tominari, Y.; Takahashi, Y.; Takeya, J.; Kitaoka, Y.; Mori, Y.; Sasaki, T. *J. Cryst. Growth* **2010**, *312*, 310−313.
(21) Matsukawa, T.; Yoshimura, M.; Uchiyama, M.; Yamagishi, M.; Nakao, A.; Takahashi, Y.; Takeya, J.; Kitaoka, Y.; Mori, Y.; Sasaki, T. *Jpn. J. Appl. Phys.* **2010**, *49*, 085502.
(22) Destri, S.; Mascherpa, M.; Porzio, W. *Adv. Mater.* **1993**, *5*, 43−45.
(23) Laudise, R. A.; Bridenbaugh, P. M.; Siegrist, T.; Fleming, R. M.; Katz, H. E.; Lovinger, A. J. *J. Cryst. Growth* **1995**, *152*, 241−244.
(24) Siegrist, T.; Kloc, C.; Laudise, R. A.; Katz, H. E.; Haddon, R. C. *Adv. Mater.* **1998**, *10*, 379−382.
(25) Della Valle, R. G.; Venuti, E.; Brillante, A.; Girlando, A. *J. Phys. Chem. A* **2008**, *112*, 6715−6722.
(26) Brillante, A.; Bilotti, I.; Della Valle, R. G.; Venuti, E.; Milita, S.; Dionigi, C.; Borgatti, F.; Lazar, A. N.; Biscarini, F.; Mas-Torrent, M.; Oxtoby, N. S.; Crivillers, N.; Veciana, J.; Rovira, C.; Leufgen, M.; Schmidt, G.; Molenkamp, L. W. *CrystEngComm* **2008**, *10*, 1899−1909.
(27) Schweicher, G.; Paquay, N.; Amato, C.; Resel, R.; Koini, M.; Talvy, S.; Lemaur, V.; Cornil, J. r. m.; Geerts, Y.; Gbabode, G. *Cryst. Growth Des.* **2011**, *11*, 3663−3672.
(28) Chen, J.; Shao, M.; Xiao, K.; Rondinone, A. J.; Loo, Y.-L.; Kent, P. R. C.; Sumpter, B. G.; Li, D.; Keum, J. K.; Diemer, P. J.; Anthony, J. E.; Jurchescu, O. D.; Huang, J. *Nanoscale* **2014**, *6*, 449−456.
(29) Yuan, Y.; Giri, G.; Ayzner, A. L.; Zoombelt, A. P.; Mannsfeld, S. C. B.; Chen, J.; Nordlund, D.; Toney, M. F.; Huang, J.; Bao, Z. *Nat. Commun.* **2014**, *5*, 3005.
(30) Schiefer, S.; Huth, M.; Dobrinevski, A.; Nickel, B. *J. Am. Chem. Soc.* **2007**, *129*, 10316−10317.
(31) Giri, G.; Li, R.; Smilgies, D.-M.; Li, E. Q.; Diao, Y.; Lenn, K. M.; Chiu, M.; Lin, D. W.; Allen, R.; Reinspach, J.; Mannsfeld, S. C. B.; Thoroddsen, S. T.; Clancy, P.; Bao, Z.; Amassian, A. *Nat. Commun.* **2014**, *5*, 3573.
(32) Diao, Y.; Tee, B. C. K.; Giri, G.; Xu, J.; Kim, D. H.; Becerril, H. A.; Stoltenberg, R. M.; Lee, T. H.; Xue, G.; Mannsfeld, S. C. B.; Bao, Z. *Nat. Mater.* **2013**, *12*, 665−671.
(33) Hiszpanski, A. M.; Loo, Y.-L. *Energy Environ.Sci.* **2014**, *7*, 592−608.
(34) Xiao, S. X.; Myers, M.; Miao, Q.; Sanaur, S.; Pang, K. L.; Steigerwald, M. L.; Nuckolls, C. *Angew. Chem., Int. Ed.* **2005**, *44*, 7390−7394.
(35) Hiszpanski, A. M.; Lee, S. S.; Wang, H.; Woll, A. R.; Nuckolls, C.; Loo, Y.-L. *ACS Nano* **2013**, *7*, 294−300.
(36) Feng, X. L.; Pisula, W.; Mullen, K. *Pure Appl. Chem.* **2009**, *81*, 2203−2224.
(37) Pisula, W.; Feng, X. L.; Mullen, K. *Chem. Mater.* **2011**, *23*, 554−567.
(38) Tremblay, N. J.; Gorodetsky, A. A.; Cox, M. P.; Schiros, T.; Kim, B.; Steiner, R.; Bullard, Z.; Sattler, A.; So, W.-Y.; Itoh, Y.; Toney, M. F.; Ogasawara, H.; Ramirez, A. P.; Kymissis, I.; Steigerwald, M. L.; Nuckolls, C. *ChemPhysChem* **2010**, *11*, 799−803.
(39) Kang, S. J.; Ahn, S.; Kim, J. B.; Schenck, C.; Hiszpanski, A. M.; Oh, S.; Schiros, T.; Loo, Y. L.; Nuckolls, C. *J. Am. Chem. Soc.* **2013**, *135*, 2207−2212.
(40) Bouchoms, I. P. M.; Schoonveld, W. A.; Vrijmoeth, J.; Klapwijk, T. M. *Synt. Met.* **1999**, *104*, 175−178.
(41) Fritz, S. E.; Martin, S. M.; Frisbie, C. D.; Ward, M. D.; Toney, M. F. *J. Am. Chem. Soc.* **2004**, *126*, 4084−4085.
(42) Mannsfeld, S. C. B.; Virkar, A.; Reese, C.; Toney, M. F.; Bao, Z. *Adv. Mater.* **2009**, *21*, 2294−2298.
(43) Yuan, Q.; Mannsfeld, S. C. B.; Tang, M. L.; Toney, M. F.; Lüning, J.; Bao, Z. *J. Am. Chem. Soc.* **2008**, *130*, 3502−3508.
(44) Krauss, T. N.; Barrena, E.; Zhang, X. N.; de Oteyza, D. G.; Major, J.; Dehm, V.; Wurthner, F.; Cavalcanti, L. P.; Dosch, H. *Langmuir* **2008**, *24*, 12742−12744.
(45) Hailey, A. K.; Hiszpanski, A. M.; Smilgies, D.-M.; Loo, Y.-L. *J. Appl. Crystallogr.* **2014**, DOI: 10.1107/S1600576714022006.
(46) Boultif, A.; Louer, D. *J. Appl. Crystallogr.* **2004**, *37*, 724−731.

(47) Mattheus, C. C.; de Wijs, G. A.; de Groot, R. A.; Palstra, T. T. M. *J. Am. Chem. Soc.* **2003**, *125*, 6323−6330.
(48) van Laake, L.; Hart, A. J.; Slocum, A. H. *Rev. Sci. Instrum.* **2007**, *78*, 083901.
(49) Avrami, M. *J. Chem. Phys.* **1941**, *9*, 177−184.
(50) Fanfoni, M.; Tomellini, M. *Nuovo Cimento D* **1998**, *20*, 1171−1182.
(51) Guo, Z.; Ma, M.; Wang, T.; Chang, D.; Jiang, T.; Wang, S. *AAPS PharmSciTech* **2011**, *12*, 610−619.
(52) Huberty, J.; Xu, H. *J. Solid State Chem.* **2008**, *181*, 508−514.
(53) Lee, S. S.; Kim, C. S.; Gomez, E. D.; Purushothaman, B.; Toney, M. F.; Wang, C.; Hexemer, A.; Anthony, J. E.; Loo, Y. L. *Adv. Mater.* **2009**, *21*, 3605−3609.
(54) Lee, S. S.; Mativetsky, J. M.; Loth, M. A.; Anthony, J. E.; Loo, Y. L. *ACS Nano* **2012**, *6*, 9879−9886.
(55) Rivnay, J.; Mannsfeld, S. C. B.; Miller, C. E.; Salleo, A.; Toney, M. F. *Chem. Rev.* **2012**, *112*, 5488−5519.